Mon. Not. R. astr. Soc. (1991) **250**, 633–637

The effects of non-coherent electron scattering on spectral line formation

K. E. Rangarajan, D. Mohan Rao and A. Peraiah
Indian Institute of Astrophysics, Bangalore 560 034, India

Accepted 1991 January 28. Received 1990 October 15

SUMMARY

We have calculated spectral line profiles from a plane-parallel homogeneous atmosphere for the complete and partial redistribution mechanisms (CRD and PRD) including coherent and non-coherent electron scattering. We find that in all the cases where the electron scattering coefficient is more than the continuous absorption coefficient, there are measurable changes in the spectral line profiles. In such situations, the PRD profiles have more emission hump compared to CRD profiles in the intermediate frequency range. We get extended wings and additional broadening of the line profiles for the case of non-coherent electron scattering compared to coherent electron scattering. These results have implications in the derivation of physical properties (for example, microturbulent velocities) of stellar atmospheres from spectral lines.

1 INTRODUCTION

Compton (1923) put forward a suggestion that the scattering of photons by electrons may account for the observed displacement of the lines in the solar spectrum towards the red near the limb. This is because the photons near the limb suffer more scatterings than those near the centre. This idea was investigated by Dirac (1925) and he derived the angle-dependent redistribution function for the electron scattering taking into account the thermal motion of electrons. He arrived at the conclusion that a shift of the lines cannot be produced by such a scattering mechanism. Chandrasekhar (1948) drew attention to the possibility of broadening lines by electron scattering. It is a well known fact that the scattering of radiation by electrons plays an important role in the atmospheres of early type stars due to the high number density of electrons. It is one of the main source of opacity in these stars. Electron scattering in spectral lines was investigated by Münch (1948), and he considered the case of a semi-infinite atmosphere in which an absorption line is formed, covered by a finite layer of electrons. With these assumptions, he obtained line profiles with shallower cores and broader wings since the photons are scattered from the continuum into the line core. His assumptions regarding the atmospheric structure were questioned by Gebbie & Thomas (1968). Auer & Mihalas (1968) considered some parametrized models in which scattering and absorption in the line, non-coherent electron scattering and absorption in the continuum all occur simultaneously. They assumed the line scattering to be described by the complete redistribution mechanism with a Doppler absorption profile. When the electron scattering coefficient exceeded continuous absorption, they obtained measurable changes in the the line profile due to electron scattering.

For strong resonance lines, one has to consider the partial frequency redistribution of photons by atoms as well as the non-coherent scattering by electrons; so the Voigt absorption profile should be employed in the calculation. We report here our study of some parametrized models in which we have incorporated the PRD and electron scattering in the spectral line calculation. We investigate the changes in the shapes of spectral lines for various parametrized models so that the underlying physics can be discerned. We (Rangarajan & Mohan Rao 1990) also studied a specific application of the effect of electron scattering on the Si II 1816 Å line in the solar chromosphere. In Section 2 we briefly describe the electron scattering function and in Section 3 we give an account of the equations and the method of solution. Section 4 contains the results and discussion and the last section, the conclusions.

2 ELECTRON SCATTERING REDISTRIBUTION FUNCTION

The angle-dependent redistribution function in the laboratory frame is given by (Mihalas 1978),

$$R^e(\nu', \boldsymbol{n}', \nu, \boldsymbol{n}) = g(\boldsymbol{n}, \boldsymbol{n}') \left[\frac{mc^2}{4\pi kT(1-\cos\theta)\nu^2}\right]^{1/2} \times \exp\left[\frac{-mc^2(\nu-\nu')^2}{4kT(1-\cos\theta)\nu^2}\right]. \quad (1)$$

This expression is valid for all wavelength region of the electromagnetic spectrum except for short wavelengths. In other words, the above formula can be applied in the limit that Compton scattering effects are negligible (i.e. $h\nu/mc^2 \leq 1$). In equation (1) ν' and ν denote the frequencies of the incoming and scattered photon, and $\boldsymbol{n}'$ and $\boldsymbol{n}$ are the incoming and scattered directions. k is the Boltzmann constant, c the velocity of light, m and T are the electron mass and temperature and θ is the scattering angle. $g(\boldsymbol{n}, \boldsymbol{n}')$ is the phase function which is normally assumed to be either isotropic or dipolar. We are giving below a brief sketch of the derivation of angle averaged electron redistribution function in the laboratory frame.

Substituting the following relations (assuming isotropic scattering)

$$w = \frac{\nu_0}{c}\sqrt{\frac{2kT}{m}}; \qquad g(\boldsymbol{n}, \boldsymbol{n}') = 1;$$

$$(1-\cos\theta) = 2\sin^2\theta/2; \qquad (\nu - \nu') = \Delta\nu,$$

we have for a normalized redistribution function,

$$R^e(\nu', \boldsymbol{n}', \nu, \boldsymbol{n}) = \frac{1}{32\pi^2 w\sqrt{\pi}} \frac{1}{\sin\theta/2} \exp\left[-\frac{(\Delta\nu)^2}{4\omega^2 \sin^2\theta/2}\right]. \tag{2}$$

The angle averaged expression can be obtained by,

$$R^e(\nu', \nu) = 8\pi^2 \int_0^{\pi} R^e(\nu', \boldsymbol{n}', \nu, \boldsymbol{n}) \sin\theta \, d\theta. \tag{3}$$

Using equation (2) in equation (3) we get,

$$R^e(\nu', \nu) = \frac{1}{2w\sqrt{\pi}} \int_0^{\pi} e^{-(\Delta\nu)^2/(4w^2\sin^2\theta/2)} \cos\theta/2 \, d\theta.$$

Let $y = \sin\theta/2$. Then we have,

$$R^e(\nu', \nu) = \frac{1}{w\sqrt{\pi}} \int_0^1 e^{-(\Delta\nu)^2/(4w^2y^2)} \, dy.$$

Let $(\Delta\nu)^2/(4w^2y^2) = z^2$. Then R becomes,

$$R^e(\nu', \nu) = \frac{1}{w\sqrt{p}} \int_{|\Delta\nu|/2w}^{\infty} \frac{e^{-z^2}}{z^2} \frac{|\Delta\nu|}{2w} \, dz = \frac{1}{w} \text{ierfc} \left|\frac{\nu' - \nu}{2w}\right|, \tag{4}$$

where ierfc is the integral of the complementary error function.

$$\text{ierfc}(z) = \int_z^{\infty} \text{erfc}(x) \, dx = \frac{1}{\sqrt{\pi}} e^{-z^2} - z[\text{erfc}(z)]. \tag{5}$$

Finally, the electron redistribution function as a function of frequencies expressed in atomic Doppler units is

$$R^e(x', x) = \left(\frac{1}{\omega}\right) \text{ierfc} \left|\frac{x - x'}{2\omega}\right|. \tag{6}$$

Here x is the frequency measured in atomic Doppler units and is given by $x = \nu - \nu_0/\Delta\nu_D$. $\Delta\nu_D$ is the Doppler width defined by the expression $\Delta\nu_D = \nu_0/c\sqrt{2kT/m}$. ω is the ratio of electron to atomic Doppler widths and is given by $\omega \simeq 43 A^{1/2}$ where A is the atomic weight of the atom under consideration. For helium atoms, ω is nearly equal to 80. Auer & Mihalas (1968) derived the angle-averaged function from first principles. It is sufficient to use the angle-averaged redistribution in most of the line profile calculations. We have used the expression given by Abramovitz & Stegun (1974) to calculate the complementary error function. The superscript 'e' denotes the electron redistribution function and 'a' for the atomic redistribution function.

In Fig. 1, the function $R^e(\beta)$ is plotted against β where $\beta = |y - y'|$ and y and y' are the frequencies expressed in electron Doppler units. Fig. 1 is in good agreement with that of Hummer & Mihalas (1967). Frequency expressed in atomic Doppler units enters in the equation of radiative transfer. So if we transform $R^e(y - y')$ to $R^e(x, x')$ we find that over a few atomic Doppler widths, $R^e(x', x)$ remains constant. Therefore the contribution from non-coherent electron scattering remains constant in the Doppler core of the line. We also see from Fig. 1 that the non-coherent electron scattering may influence the wing formation to very large atomic Doppler units away from the line centre. This is due to the large ratio of electron to atomic Doppler widths.

3 METHOD OF SOLUTION

The radiative transfer equation for a two-level atom including non-coherent electron scattering is given by

$$\pm\mu \frac{dI}{dz}(x, \pm\mu, z) = -[k_c + \sigma_e + \chi_{l_0}\phi(x)] I(x, \pm\mu, z)$$
$$+ \chi_{l_0}\varepsilon\phi(x) B + k_c B + \frac{1-\varepsilon}{2} \chi_{l_0}$$
$$\times \int_{-1}^{1} \int_{-\infty}^{\infty} R^a(x', x) I(x', \mu', z) \, dx' \, d\mu'$$
$$+ \frac{\sigma_e}{2} \int_{-1}^{1} \int_{-\infty}^{\infty} R^e(x', x) I(x', \mu', dz)$$
$$\times dx', d\mu', \tag{7}$$

where k_c and σ_e are the coefficients for continuous absorption and electron scattering per unit volume. χ_{l_0} is the atomic absorption coefficient at the line centre. ε is the probability that a photon is destroyed by collisional de-excitation following a radiative excitation. ϕ and B are the profile and Planck functions respectively. $R^a(x', x)$ and $R^e(x', x)$ denote the atomic and electron redistribution functions. For coherent electron scattering, we have

$$R^e(x', x) \, dx' = \delta(x' - x) \, dx', \tag{8}$$

where $\delta(x' - x)$ denotes the Dirac delta function. Defining

$$\beta_e = \frac{\sigma_e}{\chi_{l_0}}, \qquad \beta_c = \frac{k_c}{\chi_{l_0}} \qquad \text{and} \qquad \beta = \beta_e + \beta_c,$$

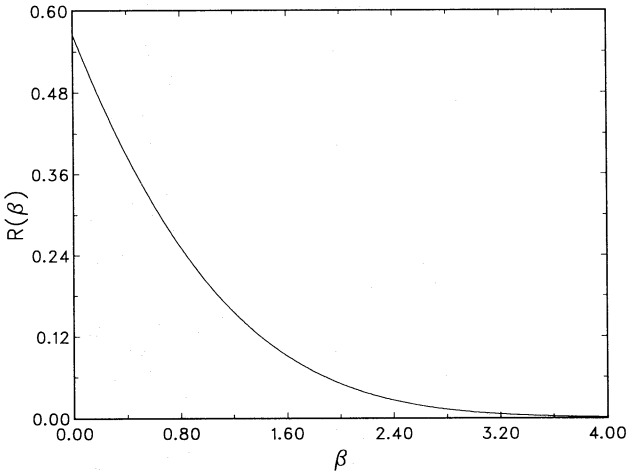

Figure 1. The angle-averaged electron redistribution function $R(\beta)$ is plotted for the case of an isotropic phase function. Here $\beta=|\nu-\nu'|/\omega$ where ν and ν' denote the absorbed and emitted frequencies of the photon in the observer's frame and ω is the ratio of electron to atomic Doppler widths.

we get

$$\pm\frac{\mu}{\chi_{l_0}}\frac{dI}{dz}(x,\pm\mu,z)=-[\beta+\phi(x)]I(x,\pm\mu,z)+\varepsilon\phi(x)B+\beta_c B$$
$$+\frac{1-\varepsilon}{2}\int_{-1}^{1}\int_{-\infty}^{\infty}R^{a}(x',x)I(x',\mu',z)\,dx'\,d\mu'$$
$$+\frac{\beta_e}{2}\int_{-1}^{1}\int_{-\infty}^{\infty}R^{e}(x',x)I(x',\mu',dz)\,dx'\,d\mu'. \qquad (9)$$

In the above equation, the first term on the right-hand side denotes the continuous absorption. The second term represents the thermal sources and the first scattering integral denotes the photons which are reshuffled within the spectral line by the atomic scattering process. The next term is the contribution from the continuous sources to the pool of photons. The second scattering integral represents the photons which are redistributed by electron scattering process. The above equation admits a symmetric solution with respect to the line centre. Therefore we need to consider only half the frequency grid, and equation (9) can be written as,

$$\pm\frac{\mu}{\chi_{l_0}}\frac{dI}{dz}(x,\pm\mu,z)=-[\beta+\phi(x)]I(x,\pm\mu,z)+\varepsilon\phi(x)B+\beta_c B$$
$$+\frac{1-\varepsilon}{2}\int_{-1}^{1}\int_{-\infty}^{\infty}[R^{a}(x',x)+R^{a}(-x',x)]$$
$$\times I(x',\mu',z)\,dx',d\mu'$$
$$+\frac{\beta_e}{2}\int_{-1}^{1}\int_{-\infty}^{\infty}[R^{e}(x',x)+R_e(-x',x)]$$
$$\times I(x',\mu',z)\,dx'\,d\mu'. \qquad (10)$$

The limits of the integration $[0,\ \infty]$ is split into two regions; i.e., $[0,\ x_1]$ and $[x_1,\ \infty]$. The second region of integration is handled analytically assuming $I_x=I_{x_1}$ for $x>x_1$ so that I_x may be taken out of the integral. Mathematically this reduces to

$$\int_{-1}^{1}\int_{0}^{\infty}[R^{e}(x',x)+R^{e}(-x',x)]I(x',\mu',z)\,dx'\,d\mu'$$
$$=\int_{-1}^{1}\int_{0}^{x_1}[R^{e}(x',x)+R^{e}(-x',x)]I(x',\mu',z)\,dx'\,d\mu'$$
$$+\int_{-1}^{1}I(x_1,\mu',z)\,d\mu'\int_{x_1}^{\infty}[R^{e}(x',x)+R^{e}(-x',x)]\,dx'$$
$$=\int_{-1}^{1}\int_{0}^{x_1}[R^{e}(x',x)+R^{e}(-x',x)]I(x',\mu',z)\,dx'\quad d\mu'$$
$$+2\left[i^2\,\mathrm{erfc}\left|\frac{x-x_1}{2\omega}\right|+i^2\,\mathrm{erfc}\left|\frac{x-x_1}{2\omega}\right|\right]\int_{-1}^{1}I(x_1,\mu',z)\,d\mu', \qquad (11)$$

where

$$i^2\,\mathrm{erfc}(z)=\int_z^{\infty}\mathrm{ierfc}(z')\,dz'=\frac{1}{2}\left[z^2+\frac{1}{2}\right]\mathrm{erfc}(z)-\frac{z\mathrm{e}^{-z^2}}{2\sqrt{\pi}}. \qquad (12)$$

The complementary error function $\mathrm{erfc}(z)$ is evaluated using the method given by Abramovitz & Stegun (1974). The integrals are reduced to summation over weighted values of the function. Equation (10) can be written at frequency x_i angle μ_j and depth z_n as

$$\pm\frac{\mu_j}{\chi_{l_0}}\frac{dI^{\pm}_{i,j,n}}{dz}=-[\beta_n+\phi_{i,n}]I^{\pm}_{i,j,n}+\varepsilon_n\phi_{i,n}B_n+\beta_{c,n}B_n$$
$$+\frac{(1-\varepsilon_n)}{2}\sum_{i'=1}^{I}\sum_{j'=1}^{J}R^{a}_{i',i}a_{i'}C_{j'}[I^{+}_{i',j',n}+I^{-}_{i',j',n}]$$
$$+\frac{\beta_{e,n}}{2}\sum_{i'=1}^{I}\sum_{j'=1}^{J}R^{e}_{i',i}a_{i'}C_{j'}[I^{+}_{i',j',n}+I^{-}_{i',j',n}], \qquad (13)$$

where $\boldsymbol{J}$ and $\boldsymbol{I}$ are the total number of angles and frequencies considered in the region of the spectral line. Adding the correction term from equation (11) to the R^e matrix we get,

$$R^{e}_{i,I}=R^{e}_{i,I}+2\left[i^2\,\mathrm{erfc}\left|\frac{x_i-x_I}{2\omega}\right|+i^2\,\mathrm{erfc}\left|\frac{x_i+x_I}{2\omega}\right|\right],\qquad x_i\le x_1. \qquad (14)$$

This problem is characterized by two frequency scales, one for the atoms and the other for the electrons. Coverage in the line must be fine enough for taking the atomic redistribution into account. Coverage in the wings should extend to four electron Doppler widths which correspond to

320 atomic Doppler widths for helium atoms. In the wings, the frequency quadrature can have a larger mesh size. We have employed a 27-point frequency quadrature between $x=0$ and $x=320$. The frequencies and the corresponding weights chosen are given in Table 1. Since the contribution from the R^a scattering integral is small beyond $x=320$, we have not included it in that region of integration.

For the angular integration, we have used two-point Gaussian quadrature. In evaluating the scattering integral over the atomic redistribution function R_{II}, we used the natural cubic-spline representation of the radiation field (Adams, Hummer & Rybicki 1971). The redistribution function R_{II} was evaluated using the procedure given by Ayres (1985). The discretized transfer equation (13) is solved using the discrete space theory technique of Grant & Hunt (1969). For more details on this technique, see Peraiah (1978). We have made necessary modifications in the code given in the above reference to solve this problem. We checked our numerical results by running the code for the same parameters considered by Auer & Mihalas (1968) and by obtaining the same results.

4 RESULTS AND DISCUSSION

Here we study the effects of electron scattering on spectral line formation from a homogeneous atmosphere. We have assumed the following boundary conditions: $I_x^+(\tau=T, \mu>0)=1$; $I_x^-(\tau=0, \mu<0)=0$ and $B(\tau)=1$. The emergent flux is plotted in Fig. 2 for an effectively thick medium with total optical thickness $T=10^6$ and $\varepsilon=10^{-4}$. We have assumed $\beta_c=0$. We have considered both CRD and PRD for comparison purposes. The curves show emission reversal except for the case of CRD without electron scattering. Lines due to CRD show more emission in the wings compared to PRD. This is due to the inhibition of photons in the wings in PRD case. This point has been discussed by several authors (Hummer 1969; Mohan Rao, Rangarajan & Peraiah 1984). PRD gives line with more peaked emission in the intermediate frequency region because the Doppler core photons are not allowed an easy diffusion into the wings. In all the cases, non-coherent electron scatterings gives extended wings compared to coherent electron scattering. This is to be expected since, non-coherent electron scattering distributes the photons from the Doppler core into the wings. Auer & Mihalas (1968) have argued from random walk principles that the wings extend to n electron Doppler widths in frequency space where the layer has an optical depth n in the electrons. The optical depth in the electrons is $n=\beta_e T$. In our case $n=10$. Coherent electron scattering gives higher flux in the intermediate frequency range and lesser flux in the wings compared to non-coherent electron scattering (compare curves 3 and 4 with 5 and 6). This is because the coherent electron scattering does not allow the core photons to diffuse to the wings whereas the non-coherent scattering admits such diffusion.

Table 1. The quadrature roots and weights chosen for the frequency integration. Frequency x_i is measured from the line centre and a_i is the corresponding weight.

x_i	a_i	x_i	a_i	x_i	a_i
0.0	0.25	4.5	0.5	30.0	10.0
0.5	0.5	5.0	0.75	40.0	15.0
1.0	0.5	6.0	1.0	60.0	20.0
1.5	0.5	7.0	1.0	80.0	30.0
2.0	0.5	8.0	1.5	120.0	40.0
2.5	0.5	10.0	2.5	160.0	40.0
3.0	0.5	13.0	3.0	200.0	50.0
3.5	0.5	16.0	3.5	260.0	60.0
4.0	0.5	20.0	7.0	320.0	30.0

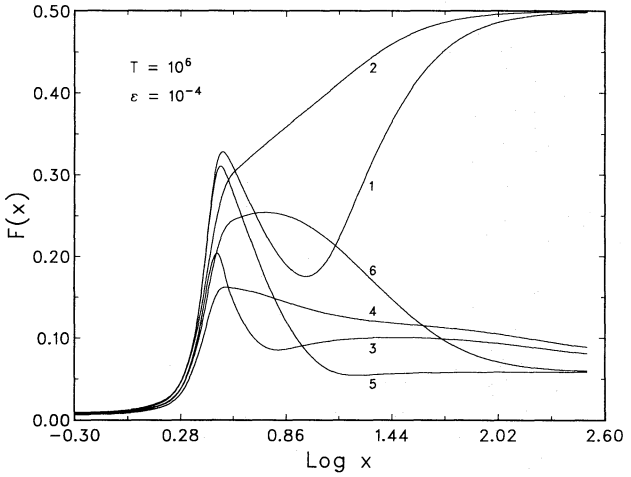

Figure 2. Emergent flux is plotted for a line with total line centre optical depth $T=10^6$ and $\varepsilon=10^{-4}$. Abscissa gives the frequency x measured from line centre in Doppler units. Odd numbers represent the results for PRD and even numbers denote the CRD values. 1 and 2 denote the results without electron scattering and 3 and 4 the results for non-coherent electron scattering with $\beta_e=10^{-5}$, where β_e is the ratio of electron scattering to line centre absorption coefficient. 5 and 6 denote the results for coherent electron scattering with the same β_e value.

The curves 1 and 2 of Fig. 3 give the emergent flux when the continuous absorption is equally important ($\beta_e=\beta_c=10^{-5}$). Now we see that the wings are totally dominated by the continuous absorption and emission processes and there is very little difference between CRD and PRD profiles. Comparing curves 1 and 2 of Fig. 3 with curves 3 and 4 of Fig. 2, we can conclude that, when the electron scattering coefficient is much more dominant than the continuous opacity coefficient in the medium, the shapes of the spectral lines are drastically affected by the presence of electron scattering.

Curve 3 of Fig. 3 represents the flux profile from a self-emitting slab with the boundary conditions $I_x^+(\tau=T, \mu>0)=0$ and $B(\tau)=1$ for the same total optical depth $T=10^6$ and $\varepsilon=10^{-4}$. The emergent flux profile which we have obtained is similar to the case where the lower boundary was illuminated. Therefore we can say that, for an effectively thick medium, the input radiation at the inner boundary does not have much effect on the emergent flux profile when non-coherent electron scattering is important. When ε is reduced to 10^{-6}, we find the emission at intermediate frequencies is reduced and we get an absorption profile (curve 4). The flux throughout the profile is less because the contribution from the thermal sources is reduced and also the non-coherent electron scattering removes the photons.

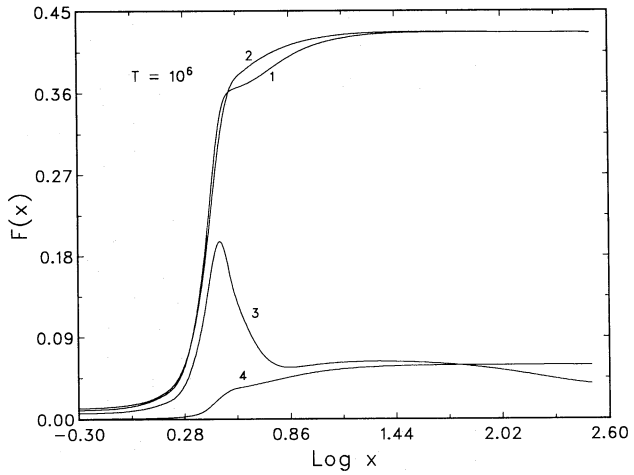

Figure 3. Emergent flux $F(x)$ is plotted against the frequency x for a line with total line centre optical depth $T=10^6$. 1 and 2 denote the results for PRD and CRD respectively for the case of a medium with $\beta_e=\beta_c=10^{-5}$ and $\varepsilon=10^{-4}$. Curve 3 represents the same case as that of curve 3 of Fig. 2 but for a self emitting medium, i.e. for a medium with no incident radiation on any one of its boundaries. Curve 4 is the same as that of curve 3 of Fig. 2 but for a medium with $\varepsilon=10^{-6}$.

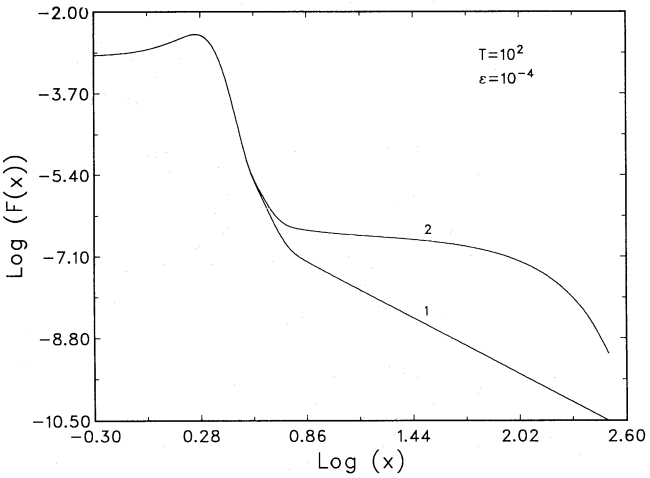

Figure 4. Curves 1 and 2 are the same as that of curves 1 and 3 of Fig. 2 but for a medium with total line centre optical depth $T=10^2$.

For an optically thin medium ($T=10^2$, $\varepsilon=10^{-4}$; Fig. 4), we obtain emission profiles. The non-coherent electron scattering gives extended wings and higher flux.

5 CONCLUSION

We find in all the cases where the ratio of electron scattering coefficient to line centre absorption coefficient is more than the ratio of continuous absorption to line centre absorption coefficient (i.e. $\beta_e>\beta_c$), the non-coherent electron scattering affects the shapes of the spectral lines and therefore should be included in the model calculations to derive more accurate diagnostics. The calculations presented in this paper show that this conclusion remains the same even if partial redistribution mechanism is important. These results may be significant for the derivation of microturbulent velocities and abundances from the spectral lines.

ACKNOWLEDGMENTS

We thank Dr F. Kneer for his useful suggestions regarding the evaluation of the R_{II} function.

REFERENCES

Abramovitz, M. & Stegun, I., 1974. *Handbook of Mathematical functions,* Dover, New York.
Adams, J. F., Hummer, D. G. & Rybicki, G. B., 1971. *J. Quant. Spectrosc. Radiat. Transfer.*, **11,** 1365.
Auer, L. M. & Mihalas, D., 1968. *Astrophys. J.*, **153,** 245.
Ayres, T. R., 1985. *Astrophys. J.*, **294,** 153.
Chandrasekhar, S., 1948. *Proc. R. Soc. Lond. A,* **192,** 508.
Compton, A. H., 1923. *Phil. Mag.*, **46,** 908.
Dirac, P. A. M., 1925. *Mon. Not. R. astr. Soc.*, **85,** 825.
Gebbie, K. B. & Thomas, R. N., 1968. *Astrophys. J.*, **154,** 285.
Grant, I. P. & Hunt, G. E., 1969. *Proc. R. Soc. London A,* **313,** 183.
Hummer, D. G., 1969. *Mon. Not. R. astr. Soc.*, **145,** 95.
Hummer, D. G. & Mihalas, D., 1967. *Astrophys. J.*, **150,** L57.
Mihalas, D., 1978. *Stellar Atmospheres,* 2nd edn, Freeman, San Francisco.
Mohan Rao, D., Rangarajan, K. E. & Peraiah, A., 1984. *J. Astrophys. Astron.*, **5,** 169.
Münch, G., 1948. *Astrophys. J.*, **108,** 116.
Peraiah, A., 1978. *Kodaikanal Obs. Bull. Ser. A,* **2,** 115.
Rangarajan, K. E. & Mohan Rao, D., 1990. *The Heating Mechanisms of Chromospheres and Coronae,* in press.